ASCE

Steel Sheet Sheathed Cold-Formed Steel Framed In-line Wall Systems. I: Impact of Structural Detailing

Amanpreet Singh, S.M.ASCE[1]; Xiang Wang[2]; Zhidong Zhang, S.M.ASCE[3]; Fani Derveni, S.M.ASCE[4]; Hernan Castaneda[5]; Kara D. Peterman, M.ASCE[6]; Benjamin W. Schafer, M.ASCE[7]; and Tara C. Hutchinson, M.ASCE[8]

Abstract: The North American construction industry has seen substantial growth in the use of cold-formed steel (CFS) framing for midrise buildings in recent years. In seismic zones, CFS-framed buildings utilize shear walls to provide the primary lateral resistance to earthquake induced loads. Although oriented strand board (OSB) and plywood panels have been traditionally used as the sheathing material for these essential components, more recently, steel sheet sheathing has emerged as a novel strategy due to its strength, ductility, ease of installation, and use of noncombustible material, among other benefits. To address the paucity of data regarding CFS-framed shear wall response within actual wall lines of buildings, a two-phased experimental effort was conducted. Wall-line assemblies were fabricated and tested with shear walls placed in-line with gravity walls. The shear walls chord stud packs include tie-rod assemblies consistent with multistory detailing. Specimens were either unfinished or finished, and the shear walls were laid out in a symmetrical or unsymmetrical fashion within in the wall line. In addition, both Type I and Type II shear wall and anchorage detailing were investigated. In this paper, the impact of test variables governing the structural detailing of CFS-framed walls are quantified through dynamic and quasi-static tests, and a companion paper presents findings regarding the impact of architectural variations on seismic performance. **DOI: 10.1061/(ASCE)ST.1943-541X.0003433.**

Introduction

The need for low-cost multihazard-resilient buildings has led to substantial growth in the use of cold-formed steel (CFS) framed construction in North American construction in recent years. CFS framing has become a popular choice for construction due to the many benefits it provides for low-rise and midrise structures. In addition to providing significant cost benefits, CFS framing produces lightweight structures with high durability and ductility. Moreover, installation costs can be low, particularly when prefabricated assemblies are used. Cold-formed steel offers a high strength-to-weight ratio and low maintenance costs due to its resistance to corrosion (Schafer 2011). Finally, CFS is inherently noncombustible, and CFS-framed buildings can potentially reduce fire spread. Despite these numerous benefits and the overall potential that CFS-framed systems have to facilitate resilient buildings, knowledge gaps in seismic performance have limited their adoption.

Buildings with repetitively framed CFS walls may develop lateral resistance through sheathing attached to the wall framing members. Sheathed CFS shear walls have commonly used oriented strand board (OSB) or plywood panels as sheathing on one or both sides of the wall. Use of steel sheets as sheathing is relatively new and offers potential benefits over other sheathing options, such as higher lateral capacity and development of well-defined ductile zones along diagonal struts prior to fastener failure. Serrette (1997) was among the first to test such walls involving specimens that were 1.22-m (4-ft) or 0.61-m (2-ft) long and 2.44-m (8-ft) high with steel sheathing of 0.46-mm (0.018-in.) and 0.68-mm (0.027-in.) thickness. These walls were loaded via a quasi-static cyclic sequential phase displacement-controlled protocol. These tests indicated that CFS shear walls using thicker sheathing resulted in larger lateral strength with walls failing through a combination of screw fasteners pulling out of the framing and tearing at the edge of the sheathing due to extensive bearing.

Yu et al. (2007) and Yu (2010) expanded and improved upon this by including 0.76-mm (0.030-in.) and 0.84-mm (0.033-in.) thickness steel options during CFS-framed shear wall testing. It was also concluded that staggered fasteners at the edge sheathing-to-stud regions helped prevent chord stud damage and improved the shear strength and ductility of the walls. Ong-Tone (2009) and Balh et al. (2014) found that reducing the fastener edge spacing led to an increase in shear strength. Moreover, shear walls with thicker steel sheet sheathing and framing members developed higher lateral resistance, with the main failure mode remaining at the sheathing to framing connections. DaBreo et al. (2014)

[1]Ph.D. Candidate, Dept. of Structural Engineering, Univ. of California, San Diego, La Jolla, CA 92093. ORCID: https://orcid.org/0000-0001-8837-2105

[2]Associate Professor, School of Civil Engineering, Sun Yat-Sen Univ., Guangzhou 510275, China; formerly, Dept. of Structural Engineering, Univ. of California, San Diego, La Jolla, CA 92093.

[3]Ph.D. Candidate, Dept. of Civil and Systems Engineering, Johns Hopkins Univ., Baltimore, MD 21218. ORCID: https://orcid.org/0000-0002-4844-7907

[4]Postdoctoral Associate, Institute of Mechanical Engineering, École Polytechnique Fédérale de Lausanne, 1015 Lausanne, Switzerland; formerly, Dept. of Civil and Environmental Engineering, Univ. of Massachusetts, Amherst, MA 01003. ORCID: https://orcid.org/0000-0001-8159-0345

[5]Ph.D. Candidate, Dept. of Civil and Environmental Engineering, Univ. of Massachusetts, Amherst, MA 01003.

[6]Associate Professor, Dept. of Civil and Environmental Engineering, Univ. of Massachusetts, Amherst, MA 01003.

[7]Professor, Dept. of Civil and Systems Engineering, Johns Hopkins Univ., Baltimore, MD 21218.

[8]Professor, Dept. of Structural Engineering, Univ. of California, San Diego, La Jolla, CA 92093 (corresponding author). ORCID: https://orcid.org/0000-0001-9109-7896. Email: tara@ucsd.edu

Note. This manuscript was submitted on September 2, 2021; approved on April 18, 2022; published online on September 22, 2022. Discussion period open until February 22, 2023; separate discussions must be submitted for individual papers. This paper is part of the ***Journal of Structural Engineering***, © ASCE, ISSN 0733-9445.

improved the chord stud design by introducing blocking members that reduced stud twisting and increased wall lateral strength. Shamim et al. (2013) dynamically tested single- and double-story CFS-framed steel sheet sheathed shear walls and showed that the failure modes and seismic performance of dynamically tested walls were consistent with observations from monotonically and reverse cyclically tested shear walls in the literature. These were the first experiments that evaluated the seismic performance of steel sheet sheathed CFS-framed shear walls through shake table testing.

Recent studies by Rizk and Rogers (2017), Santos and Rogers (2017), and Briere and Rogers (2017) have attempted to bridge the gap between the lateral capacities of steel sheet sheathed CFS-framed and hot-rolled steel shear walls through development of center-sheathed specimens, termed midply shear walls, in which a single piece of steel sheathing is sandwiched between built-up studs. These specimens attained shear resistances as high as 165 kN/m (11.3 kips/ft), more than four times the largest strength values for design available in AISI S400-15 (AISI 2015b), while also demonstrating ductile behavior at large lateral drifts (7%). The higher shear resistance found in the center-sheathed wall design was attributed to avoiding sheathing pull-through within the fastener connection, which aligns well with the findings from a recent study by Zhang et al. (2021) on the performance of fastener connections adopted in the center-sheathed shear walls under cyclic loading.

Research conducted by these and several other authors have contributed to the development of the current North American standards, AISI S100-16 (AISI 2016), AISI S240-15 (AISI 2015a), and AISI S400-15 (AISI 2015b), providing guidelines for design of shear walls with steel sheet sheathing. Although these current standards can be used to design CFS shear walls to meet the seismic demands for low-rise to midrise (3–6 story) buildings, design guidelines for midrise and high-rise buildings taller than 6 stories are lacking due to their large lateral load resistance requirements.

Despite the available experimental data and advancement of design standards, additional limitations exist. Notably, thus far, only Shamim et al. (2013) have incorporated dynamic loading during their experiments on steel sheet sheathed CFS-framed shear walls. In contrast, most prior programs have involved testing shear walls under quasi-static monotonic or reversed cyclic loading. An additional and equally important limitation within the experimental literature is that the previous studies have considered shear walls and gravity walls separately. However, these wall components are generally placed along the same line for architectural purposes and thus may be subject to similar kinematic demands. Moreover, walls often have openings (doors and windows) and have finishes installed (exterior and interior) for insulation purposes. Structurally accounting for these openings involves assuming a load path around the opening, thus creating frame action. The tension and compression developed during lateral loading is resolved at the extreme wall ends. This concept, referred to as Type II wall detailing emerged from testing of 12-m-long shear walls with openings (Steel Framing Alliance 1997).

Despite these and other test programs, the understanding of CFS wall-line structural behavior, particularly the contribution from non-designated systems such as gravity walls, under seismic events remains limited. In addition, continuous tie-rod systems have emerged as popular tie-down systems in midrise (3–6 story) CFS-framed buildings. This tie-down system provides a continuous load path from the floors to the walls and into the foundation. A continuous tie-down system can be used in a multistory building to resist overturning forces and ensure structural stability and integrity. Although the construction industry has moved ahead with its adoption, testing to support code provisions for their inclusion has lagged because most prior CFS shear walls testing has employed hold-downs as the traditional tie-down system.

The experimental program in the current research project was designed to include test variables that address several of the aforementioned limitations in an effort to enrich the experimental database documenting the performance of steel sheet sheathed CFS-framed wall assemblies. In this paper, the impact of test variables governing the structural detailing of CFS-framed walls is discussed. In particular, the impact of detailing such as tie-down and anchorage system on wall behavior has been quantified through a series of dynamic and quasi-static tests. In a companion paper (Singh et al. 2022b), the impact of detailing such as window opening and unsymmetrical shear wall layout on steel sheet sheathed CFS wall-lines are the focus. Usually ignored in design applications, the beneficial effects of nonstructural finish application on several wall performance metrics are also discussed in detail in the companion paper. Interested readers are referred to Singh et al. (2022b) to understand the effects of architectural/nonstructural details, which form a significant portion of the current research findings.

Experimental Program

A two-phased experimental program was undertaken to advance the understanding of CFS-framed steel sheet sheathed shear walls. Coined the CFS-NHERI project, this experimental program within the project had the following primary objectives: (1) characterize the dynamic performance of CFS walls that include shear walls and gravity walls, i.e., wall lines; (2) understand the effect of finishes on wall behavior; (3) compare the behavior of Type I and Type II wall lines; (4) compare the wall behavior with steel tension tie-rods assembly with that of hold-down tie-down systems; (5) compare the behavior of symmetrical and unsymmetrical wall lines; (6) understand the effect of openings on wall behavior; and (7) examine lateral load sharing between shear walls placed in-line with gravity walls.

The first phase of the experimental program was conducted at the NHERI Large High-Performance Outdoor Shake Table (LHPOST) at the University of California, San Diego (Van Den Einde et al. 2004). Shear walls placed in-line with gravity walls carrying tributary mass were tested at full scale, first under a sequence of increasing-amplitude (in-plane) earthquake motions, and subsequently under slow monotonic pull conditions (for select specimens). Pairs of eight nominally identical wall configurations, resulting in 16 walls in total, were tested during the shake table test program. Each specimen was a wall line with a varying configuration of shear wall and gravity wall segments placed in-line with each other. The shear wall segments were detailed with tie-down assemblies consisting of compression stud packs and tension tie-rods with a single steel sheet installed as sheathing on one side.

The selection of wall details was motivated by a designed CFS archetype building (4 and 10 stories) harmonized with available experimental data (Singh et al. 2020a). Selected details reflect the shear and gravity detailing from approximately the midheight floors within the 10-story building or bottom floor of a 4-story building. Compression stud packs with tension tie-rods, a common detail seen in multistory building design, provided wall overturning and uplift restraint. The various configurations in the test matrix included specimens in an unfinished or finished, symmetric or unsymmetrical, Type I or Type II shear wall detailing configuration, and with or without a window opening.

The second phase of the experimental program was conducted at the University of California, San Diego, Structural Engineering Powell Laboratory. In this phase, 10 single wall-line configurations were tested under quasi-static cyclic displacement-controlled

loading conditions. Although wall configurations were of similar geometry to those tested in the shake table phase, single walls were tested rather than pairs, and a quasi-static displacement controlled protocol at the wall top was imposed, rather than a dynamic base excitation. Two wall configurations tested during the shake table test program were repeated in the quasi-static test program. In total, 16 unique wall configurations were tested between the two test phases.

Shake Table Test Phase

Test Matrix and Setup

The CFS-NHERI wall-line shake table phase consisted of eight wall configurations tested in nominally identical wall pairs, amounting to 16 wall specimens in total (Table 1). Specimen names refer to the characteristics of each 1.22-m (4-ft) quadrant length of the 4.88-m (16-ft) specimen appended with a number indicating whether it was a Type I or Type II wall system as defined by AISI S400-15 (AISI 2015b), specifying the locations of tension tie-rods. For example, SGGS-1, which is the baseline specimen, is a Type I **S**hear-**G**ravity-**G**ravity-**S**hear wall-line specimen with a pair of tie-rods at each shear wall segment end, and SWWS-2 is a Type II shear-window-window-shear wall-line specimen with tension tie-rods located at the wall ends. The wall-line specimen geometry was held consistent as 4.88-m (16-ft) in length and 2.74-m (9-ft) in height. The baseline specimen was an unfinished wall with a 2.44-m gravity wall segment in the middle bookended by 1.22-m-long Type I shear wall segments. The Type I shear wall segment was detailed with a pair of tie-down assemblies consisting of compression stud packs built up by welded toe-to-toe 600S250-97 stud members [AISI S100-16 (AISI 2016)] and a ϕ29-mm (ϕ1-1/8 in.) Grade B7 tension tie-rod (measured yield point at 877 MPa) in the middle of the stud packs. The all-thread tie-rods were provided with a Grade 8 ϕ29-mm (ϕ1-1/8 in.) coupler at approximately midheight of the wall, simulating a continuous floor to roof connection. The shear wall segments were sheathed on their exterior face with 0.76-mm (0.030-in.) sheet steel of ASTM (2017) Grade 230 MPa (33 ksi) nominal yield strength. The steel sheet was attached to the wall framing using No. 12 gauge 22-mm (7/8-in.) flat pan-head screws at 51-mm (2-in.) on center (o.c.) edge (or 102-mm staggered equivalent) and 305-mm (12-in.) o.c. field spacing.

The gravity wall framing utilized 600S250-68 stud members placed at 610 mm (2 ft) o.c. The top and bottom tracks were constructed of continuous 600T250-97 members. Additionally, a 1200T250-97 ledger track was attached to the top 0.3-m (12-in.) height of the interior face of the wall with six rows of screws at 51-mm (2-in.) o.c. [Fig. 1(a)]. The bottom four rows used No. 12 gauge 22-mm (7/8-in.) flat pan-head screws, and the top two rows used No. 12 gauge 38-mm (1 − 1/2-in.) hex-head screws because those screws were required to penetrate a longer distance due to the presence of three layers of steel framing. The walls were fully blocked, with bracing and blocking installed at third height points. All framing members were ASTM (2017) Grade 345 MPa (50 ksi) nominal strength and were assembled using No. 10 gauge 19-mm (3/4-in.) flat pan-head screws.

Fig. 1 shows the framing details of the baseline wall specimen (SGGS-1) as installed in the test setup. Similar components were used for the fabrication of all other wall specimens. These wall

Table 1. Test matrix and definition of specimens

Test phase	Specimen	Description	Tie-down detailing	Shear wall detailing	Finish	
					Exterior face	Interior face
Shake table test phase (two each)	SGGS-1	Baseline specimen. Symmetrical shear segments on both wall ends	Tension tie-rods	Type I	—	—
	SGGS-1XS	SGGS-1 with finer steel sheet fastener pattern	Tension tie-rods	Type I	—	—
	SGGS-1F	SGGS-1 with finish	Tension tie-rods	Type I	EIFS	Gypsum
	SGGS-1SB	SGGS-1 with composite steel sheet glass-mat panels	Tension tie-rods	Type I	EIFS	Gypsum
	SGGS-2B	SGGS-2 with coarser steel sheet fastener pattern	Tension tie-rods	Type II	—	—
	SGGG-1	Unsymmetrical wall: shear segment on one wall end only	Tension tie-rods	Type I	—	—
	SWWS-1	SGGS-1 with window opening in the middle bays	Tension tie-rods	Type I	—	—
	SWWS-2	SGGS-2 with window opening in the middle bays	Tension tie-rods	Type II	—	—
Quasi-static test phase (one each)	SGGS-2	Symmetrical: shear segments on both wall ends	Tension tie-rods	Type II	—	—
	SGGS-2F	SGGS-2 with finish	Tension tie-rods	Type II	EIFS	Gypsum
	SWWS-1	SGGS-1 with window opening in the middle bays	Tension tie-rods	Type I	—	—
	SWWS-2	SGGS-2 with window opening in the middle bays	Tension tie-rods	Type II	—	—
	SWWS-2F	SWWS-2 with finish	Tension tie-rods	Type II	EIFS	Gypsum
	SGGG-1F	SGGG-1 with finish	Tension tie-rods	Type I	EIFS	Gypsum
	SGGS-1HD	SGGS-1 with hold-downs	Hold-downs	Type I	—	—
	SGGS-1HDF	SGGS-1HD with finish	Hold-downs	Type I	EIFS	Gypsum
	GGGG	Gravity frames in all bays	None	N/A	—	Gypsum
	GGGG-F	GGGG with exterior finish	None	N/A	EIFS	Gypsum

Note: Specimen names indicate characteristics of each quadrant length appended with a number for shear wall detailing and additional characters for differences in finish, fastener detail, tie-down detail. EIFS = exterior insulation finishing system.

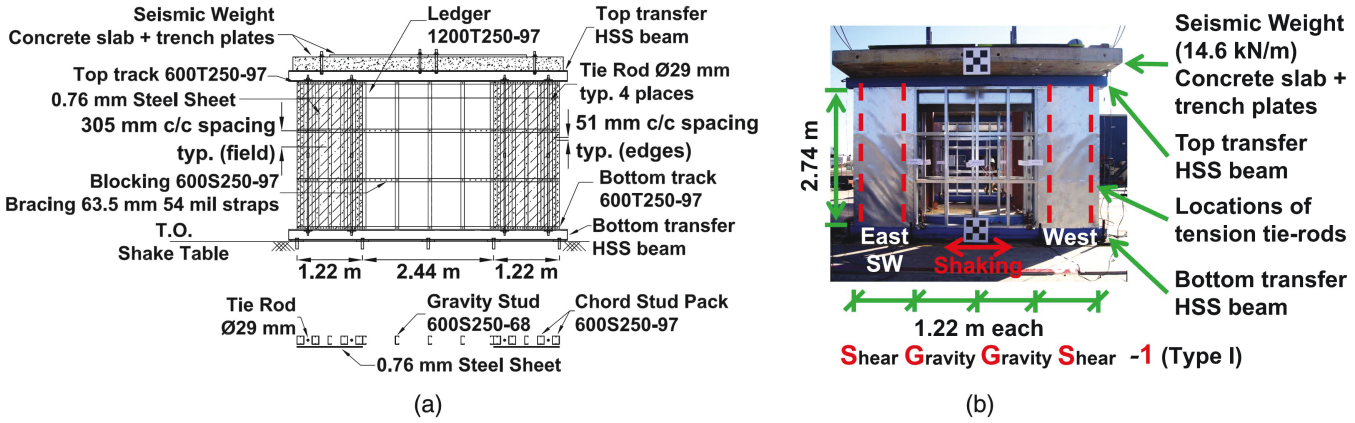

Fig. 1. Baseline Specimen SGGS-1: (a) framing details; and (b) as installed on shake table.

details were motivated from a CFS-framed archetype building designed according to current code guidelines and utilizing recently available experimental data. Selected shear wall details reflected the detailing from approximately the midheight floors within a 10-story building situated in a high seismic region (Singh et al. 2020a).

For specimens requiring finish application, gypsum boards on the interior face and glass-mat sheathing panels with Exterior Insulation Finishing System (EIFS) on the exterior face were installed in the field using No. 8 gauge 44-mm ($1-3/4$-in.) flat head screws at 152-mm (6-in.) o.c. edge and 406-mm (16-in.) o.c. field spacing. Installed gypsum boards were 1.22-m (4-ft) × 2.44-m (8-ft) × 16-mm (5/8 - in.) Firecode Type X, and glass-mat sheathing panels were 1.22-m (4-ft) × 2.74-m (9-ft) × 16-mm (5/8 - in.) Firecode Type X. Singh et al. (2022b) provides a description of the steps involved in the finish application.

The NHERI at University of California, San Diego, shake table footprint of 12.2-m (40-ft) × 7.6-m (25-ft) allowed for two pairs of nominally identical walls to be tested simultaneously. The specimens were installed by attaching the specimens to top and bottom steel load transfer beams using two rows of 12.7-mm (0.5-in.) A325 shear bolts (ASTM 2014). These transfer beams were 5.2-m (17-ft) in length, 203.2-mm (8-in.) × 203.2-mm (8-in.) × 15.9-m (0.625-in.) square hollow structural section HSS A500 steel tubes [ASTM A500/A500M-18 (ASTM 2018)]. The two wall pairs were provided with temporary out-of-plane bracing to ensure the walls remained vertical during the top mass installation. Prior to mass installation, tension tie-rods were installed and tightened using access holes in the transfer beams with a nut-plate assembly bearing against the inside surfaces of the top and bottom beams. Fig. 2 shows an elevation view of the tension tie-rod assembly when installed in the test setup.

The concrete mass slabs (5.0 m × 3.0 m × 254 mm) were placed atop the wall pairs and post-tensioned to the top transfer beams. Additionally, two steel trench plates (1.8 m × 3.0 m × 38 mm each) were installed and post-tensioned to the concrete slab on each wall pair to achieve the desired seismic weight of 14.6 kN/m (1,000 lb/ft) per wall. This gravity load was estimated to be typical for CFS-framed buildings (Singh et al. 2020a) and also fell in the range of gravity loads [8.3 kN/m (570 lb/ft) to −18.2 kN/m (1,250 lb/ft)] considered in past research on combined gravity and lateral loading of shear walls (Hikita 2006). The input earthquake motions were applied in the east–west direction using the single-axis shake table, which aligned with the longitudinal axis of the wall specimens. Fig. 3 shows the top and isometric view of the completed test setup.

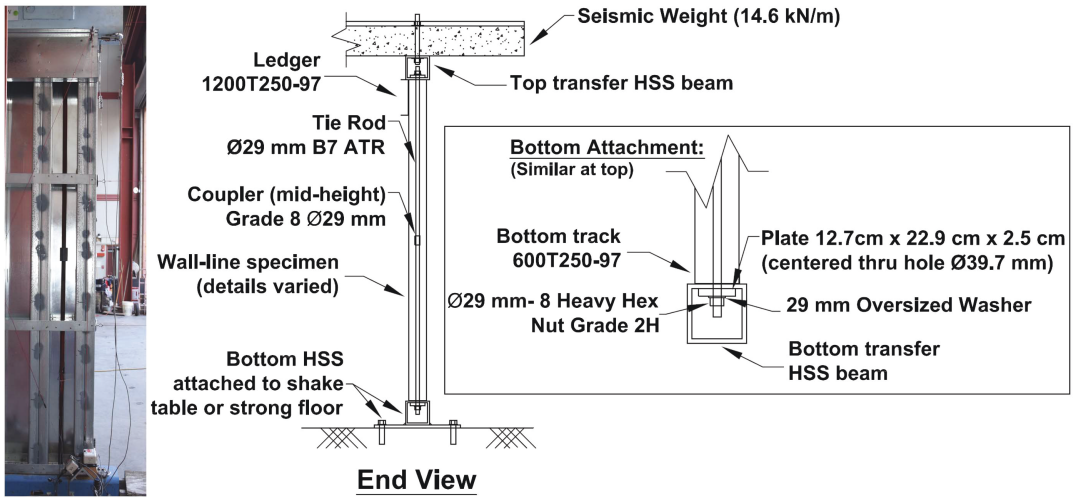

Fig. 2. Elevation view of interior face of wall showing tension tie-rod assembly.

Test Protocol and Instrumentation

The wall specimens were tested under a sequence of increasing-intensity earthquake motions. Select wall specimen pairs were also tested under slow monotonic pull conditions with a target of attaining a 40% postpeak strength degradation. Two test motions from two different earthquake events, namely the (1) 1994 $M_w = 6.7$ Northridge earthquake (Canoga Park record component ID: CNP196); and (2) 2010 $M_w = 8.8$ Maule earthquake in Chile (Curicó record component ID: CUR EW) were selected as seed motions in this test program. These motions were selected in part to assure representative strong earthquakes from past California events, while also including an event with a long duration of strong shaking. The characteristics of the selected seed motions are given in Table 2 and Fig. 4.

To facilitate measurement and observation of the seismic behavior of the specimens and obtain their dynamic characteristics at different performance levels, as described in Table 3, a unique scaling strategy was developed. The test arrangement, although beneficially subjecting two pairs of specimens to the same input motion, also required the specimens selected for simultaneous testing to be selected such that they had similar expected lateral strength and initial stiffness. In this regard, the scaled earthquake motions imposed on the two wall pairs would achieve similar target performance levels. However, when such a pairing was not possible, the motion scaling strategy had to take into account the strength and stiffness differences between the two wall pairs to be tested simultaneously.

Complementing the earthquake test sequence, low-amplitude white-noise tests with root-mean square (RMS) intensities of 1.5%g and 3%g and 4-min duration were conducted before and after each earthquake test to determine the dynamic characteristics of the wall specimens at different damage stages. The measured natural period of the two wall pairs within the test group, determined from the 3%g RMS white-noise test, were used to calculate the scale factor for the subsequent earthquake test. Scale factors of the motions aimed to achieve the intended target performance levels that progressively damage the wall specimens (Table 3). The developed motion scaling procedure, which used pretest benchmark model predictions and measured natural period of specimens at different damage stages during the testing sequence, has been discussed in detail by Singh et al. (2021b).

The two pairs of wall specimens concurrently on the table were densely instrumented with more than 120 analog sensors connected to a multinode distributed data-acquisition system that sampled data at a rate of 256 Hz. These analog sensors included (1) accelerometers measuring top mass and shake table accelerations, (2) string potentiometers measuring top mass and table displacements as well as wall sheathing panel shear distortion, (3) strain gauges measuring tension tie-rod strains, and (4) linear potentiometers measuring wall uplift. A pair of two vertical and two diagonal

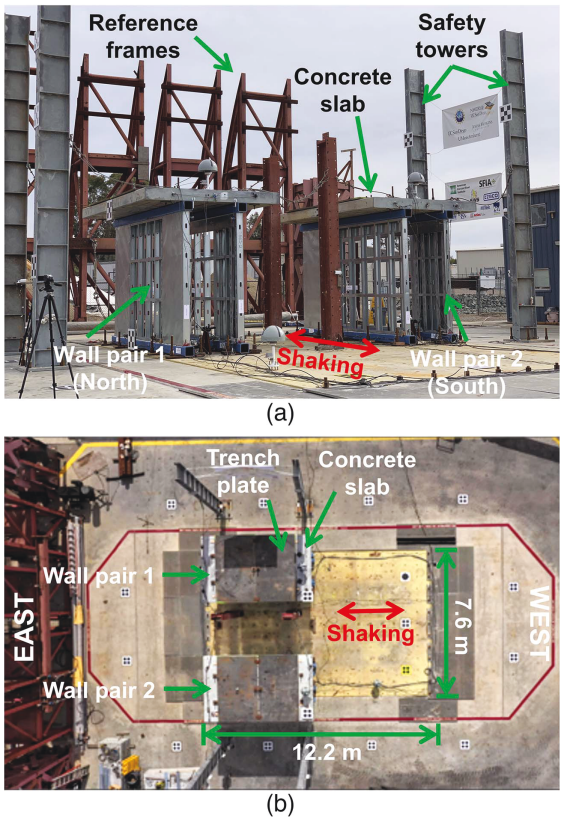

Fig. 3. Shake table test setup: (a) isometric view; and (b) top view.

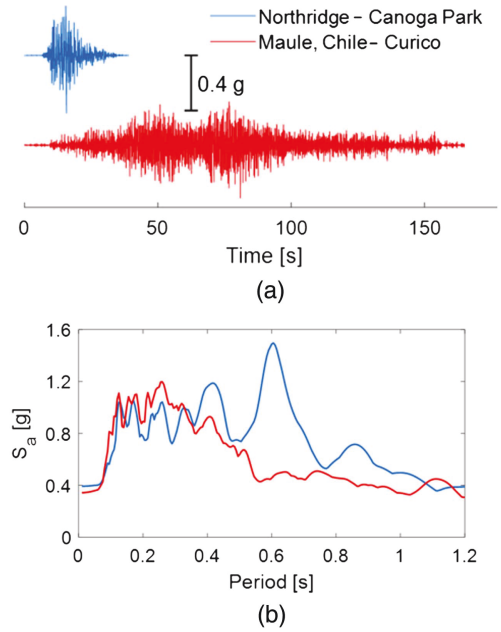

Fig. 4. Selected earthquake seed motions: (a) acceleration time histories; and (b) elastic pseudo-acceleration spectra ($\xi = 5\%$).

Table 2. Characteristics of selected seed motions

Record ID	Earthquake event, location	Year	M_w	Station	Component direction	R_{rup} (km)	PGA (g)	PGV (cm/s)	PGD (cm)	Ds_{5-95} (s)
CNP196	Northridge, California	1994	6.7	Canoga Park	East–west	14.7	0.39	60.4	12.5	10.6
CUR-EW	Maule, Chile	2010	8.8	Curicó	East–west	N/A	0.41	32.6	5.2	51.6

Note: PGA = peak ground acceleration; PGV = peak ground velocity; and PGD = peak ground displacement.

Table 3. Target performance level definition

Target performance level	Response characteristics	Force target, V_{target} ($\%V_u$)	Drift target, Δ_{target} ($\%\Delta_{Vu}$)	Damage
Elastic	Linear	20%–40%	~20%	Minimal
Quasi-elastic	Quasi-linear	60%–70%	30%–40%	Minor (cosmetic)
Design	Nonlinear	Near strength	75%–95%	Moderate
Above design (optional)	Noticeable pinching	<20% strength deterioration	125%–150%	Major; uncompromised structural integrity

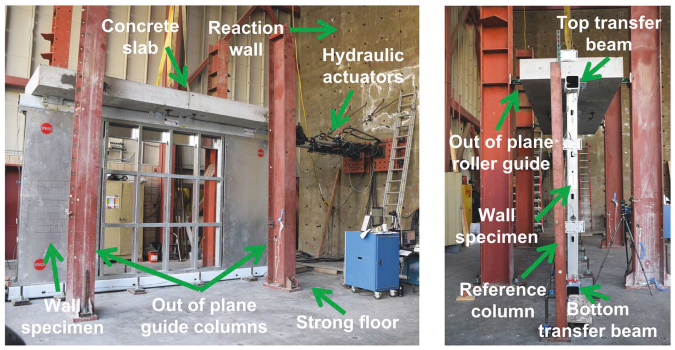

Fig. 5. Quasi-static cyclic test setup: (a) isometric view; and (b) end view.

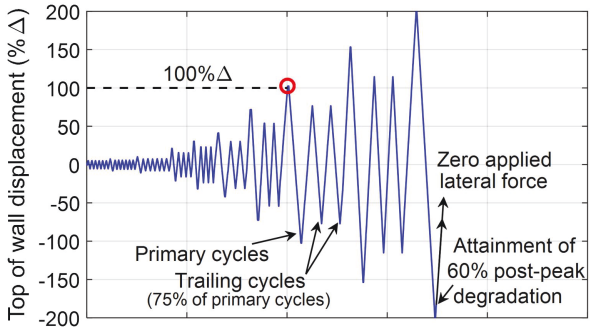

Fig. 6. CUREE protocol adopted in quasi-static test phase.

string potentiometers in a double-triangle configuration were used to evaluate the wall panel shear distortion by measuring the change in angles of the triangles. A pair of colocated strain gauges installed on the tie-rods were used to calculate axial forces in the rods. Detailed expressions used in these panel distortion and axial force calculations can be found in Singh et al. (2021b). Additionally, a Global Positioning System (GPS) and remote sensing equipment, including unmanned aerial vehicles (UAVs) and light detection and ranging (LiDAR) system, were employed to collect digital data during the construction and testing phases. Finally, an array of 15 high-resolution cameras were used to record the wall response during the tests documenting any physical damage.

Quasi-Static Cyclic Test Phase

The CFS-NHERI wall-line quasi-static cyclic test phase consisted of 10 single wall configurations tested in the University of California, San Diego, Structural Engineering Powell Laboratory. The test setup was similar to the shake table test setup, with the same HSS top and bottom load-transfer beams used for anchoring the wall to the reaction floor and transferring lateral load via a pair of double-acting hydraulic actuators with a 220-kN (50-kip) load capacity and ± 60 cm (± 23.6 in.) stroke. Fig. 5 shows a wall specimen as installed in the quasi-static test setup.

Two concrete slabs (2.44 m × 1.52 m × 305 mm each) were used to apply a total of 12.4 kN/m (850 lb/ft) gravity load. Different from the shake table test phase, single walls were tested, with out-of-plane stability of the specimens provided via columns with roller guides at the top mass location to assure restraint from movement in the transverse direction. The 10 wall configurations tested in this phase of the program are listed in Table 1. Specimen names follow the convention adopted during the shake table test program, namely referring to the characteristics of each 1.22-m quadrant length of the 4.88-m long specimen appended with a number indicating whether it is a Type I or Type II wall system. Five configurations in this test program had finishes applied in the field after installation of the specimens into the test setup. In general, all wall configurations used tension tie-rods for shear wall detailing, of either a Type I and Type II detailing. However, two configurations in the quasi-static test program, namely SGGS-1HD and SGGS-1HDF, were detailed instead with hold-downs at the ends of each shear wall. The configurations GGGG and GGGG-F, as the naming convention suggests, were detailed as gravity walls with no tie-downs, without and with finish, respectively.

The walls were subjected to a displacement-controlled reversed cyclic CUREE protocol (Krawinkler et al. 2001) as shown in Fig. 6. The reference displacement required to define this protocol was obtained from the wall-line behavior measured during the shake-table experiments, namely $\Delta = 2\%$ as measured for Specimen SGGS-1. The specimens were reverse cyclically tested until a 60% postpeak lateral strength drop was observed. Subsequently, the test was concluded by returning the specimen to zero applied lateral force. Similar to the shake table setup, the wall specimens were densely instrumented in this case with more than 40 analog sensors measuring wall lateral drift and load as well as wall local measurements such as sheathing panel shear distortion, tension tie-rod strains, and wall uplift. Complementing the analog sensors, five high-resolution cameras also recorded the wall response during the tests. Further details regarding the quasi-static cyclic test program are available in Singh and Hutchinson (2022).

Results and Discussion

In this section, the impact of test configuration variables pertaining to the structural detailing is discussed by comparing select groups of specimens systematically. First, however the performance of the baseline Specimen SGGS-1 is discussed. Based on the wall details chosen from the designed CFS archetype building and industry partners' input, the Specimen SGGS-1 was selected as the baseline specimen. This specimen was designed as an unfinished symmetric configuration, a 2.44-m (8-ft) gravity wall segment in the middle, and 1.22-m (4-ft) Type I shear wall segments on each end, which

used compression chord stud packs with a steel tension tie-rods assembly. This also allowed for direct cross-comparisons with other wall configurations that were finished, or had an unsymmetrical configuration, or were designed as Type II shear walls, or used traditional hold-downs as tie-downs in conjunction with chord stud packs.

Baseline Specimen Performance

The baseline Specimen SGGS-1 wall pair was subjected to four earthquake motions with increasing intensity, as listed in Table 4, as well as a sequence of low-amplitude white-noise tests before and after each earthquake test. Following the completion of the dynamic test sequence, this wall pair was also subjected to static monotonic displacement loading by restraining the top of the specimen and moving the base of the shake table slowly in an effort to capture its postpeak behavior at large displacements. Fig. 7 shows the force-displacement responses of the wall specimen during the earthquake tests and the subsequent monotonic pull test.

This specimen's response was essentially linear for the first three earthquake tests, with less than 0.4% achieved drift ratio and a lateral force below 50% of strength. Physical damage to the wall specimen was also very minimal during these lower intensity elastic (EQ1: E1 and EQ2: E2) and quasi-elastic (EQ3: QE) level earthquake tests as the walls underwent low drift demands. Less than 2% of the screw fasteners showed incipient bearing into the steel sheet with only a minor low tilt angle. No damage was seen in any framing members. Nonetheless, transient elastic sheet buckling could be observed and heard as it cycled within the tension field during the dynamic shaking. The specimen demonstrated nonlinearity during the design earthquake test (EQ4: DE) when the drift demand reached 1% and the specimen experienced lateral forces up to 85% of its strength. Buckling of the steel sheet with a widely distributed tension field and readily observable lines of plastic deformation were visible at the end of this test. Fastener tilting and bearing onto the steel sheet was evident in approximately 20% of the screws following the test, with most clustered at the corners of the steel sheet directly along the main diagonals of the tension field.

During the monotonic pull test, the specimen reached strength V_u at 160.2 kN (36.0 kip) at a drift ratio Δ_{Vu} of 1.95% and during continued pull demonstrated a postpeak degradation of 40% at 4.15% drift ratio. The elastic stiffness of the specimen, K, defined as the secant stiffness at 40% strength, was measured as 83.0 kN/cm (47.4 kip/in.). Compared with a 1.22-m long Type I isolated shear wall with 0.76-mm (0.030-in.) steel sheet sheathing and 51-mm (2-in.) o.c. fastener edge spacing from AISI S400-15 (AISI 2015b), the baseline Specimen SGGS-1 demonstrated 3.3 times higher lateral strength. Most of the damage in the SGGS-1 wall pair occurred during the monotonic pull, when extensive shear buckling of the steel sheet was observed as the width of the tension field increased with increasing drift demand, widening to include most of the steel sheet sheathing. At the end of the monotonic pull test, local buckling of the gravity stud adjacent to the shear segment compression stud pack at diagonally opposite locations of the gravity wall segment was observed. However, the compression stud packs and track framing members did not experience any visible damage.

At the end of the test, most steel sheet screws showed some form of damage. Sheet pull over or edge tearing extended from the corner to quarter height of the chord studs and a third of the length of the top and bottom tracks, with damage also to a few field screws in the middle of the sheet. Outside of the heavily damaged diagonal tension field, fasteners along the off-diagonals showed some tearing of the sheet steel as screws tilted to large angles. Fasteners furthest away from the plastic tension field region showed bearing/tilting damage accumulated primarily during the earthquake tests. Fig. 8 shows these physical damage observations. All of the connection damage modes seen in the wall-line tests were also observed in steel sheet to CFS framing member connection tests performed by Zhang and Schafer (2020). The accumulation of damage through the earthquake test sequence led to an elongation of the fundamental period from 0.157 s in its undamaged state to 0.199 s following the design-level earthquake test EQ4. Similarly, the damping ratio increased from 2.1% in its undamaged state to 5.3% after earthquake test EQ4. Based on the results of the baseline

Table 4. Selected scaled earthquake test motions and association with target performance level (Specimen SGGS-1)

Test motion ID	Target performance level	PGA (g)	PGD (cm)
EQ1: CNP196	Elastic (E1)	0.31	7.69
EQ2: CUR-EW	Elastic (E2)	0.24	2.32
EQ3: CNP196	Quasi-elastic (QE)	0.66	17.66
EQ4: CNP196	Design event (DE)	1.20	35.0

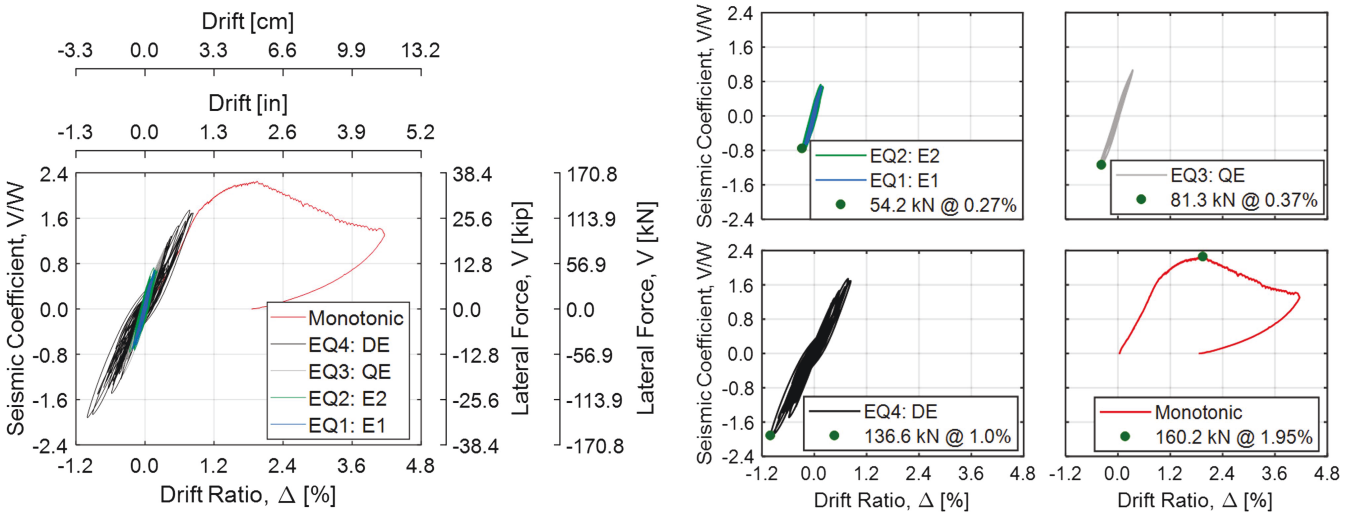

Fig. 7. Force-displacement response of baseline Specimen SGGS-1.

J. Struct. Eng., 2022, 148(12): 04022193

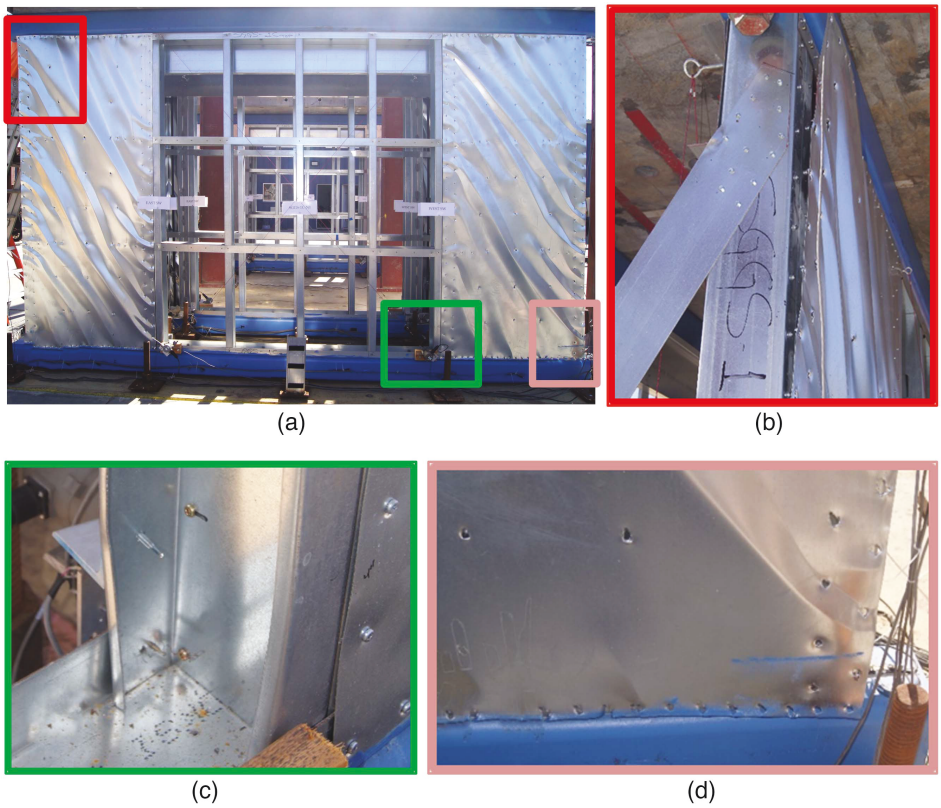

Fig. 8. Physical damage to Specimen SGGS-1 following the end of monotonic test ($\Delta_{res} = 1.86\%$): (a) tension field in steel sheets; (b) sheet pullover; (c) local buckling of gravity stud; and (d) screw edge tearing.

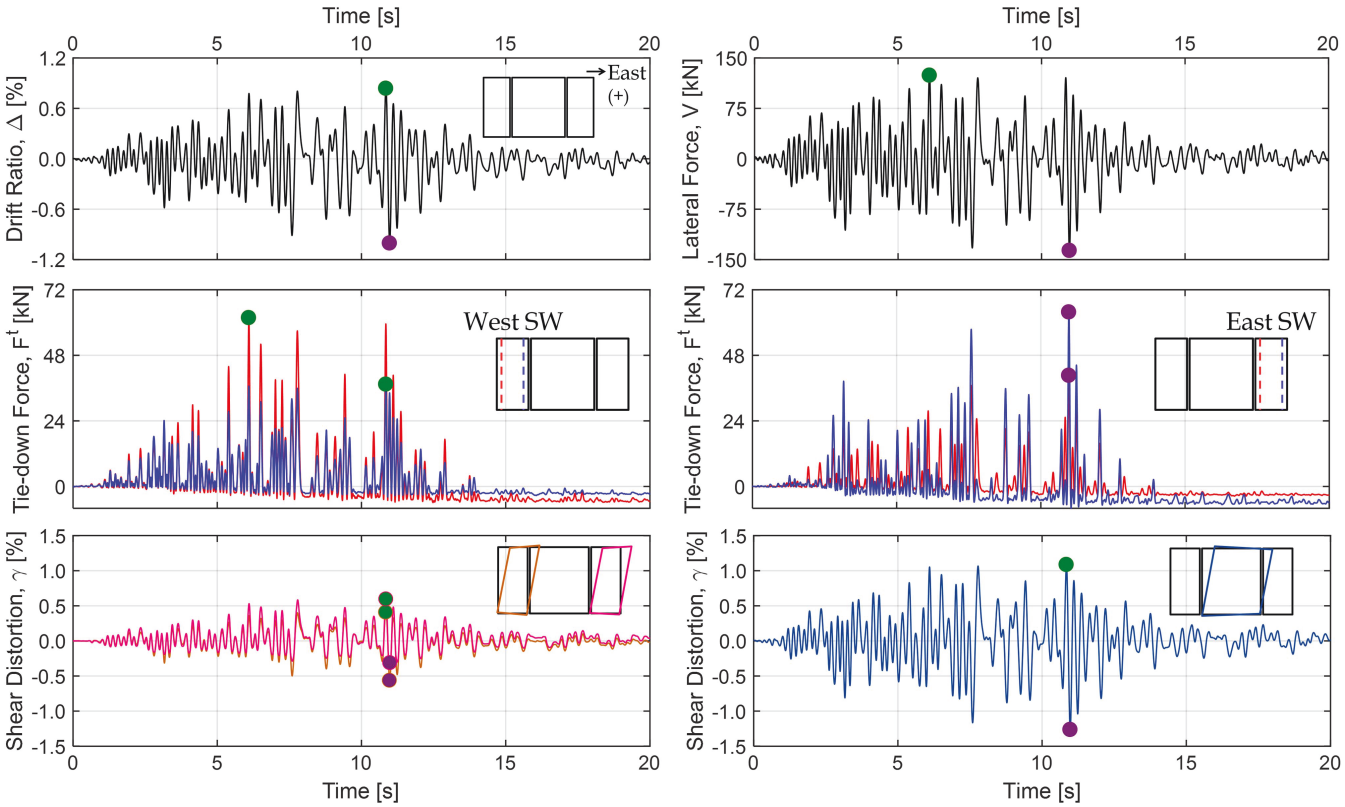

Fig. 9. SGGS-1 specimen local response during earthquake test EQ4: DE. Schematics within subplots indicate location and type of response plotted. Symbols denote peak in the two drift directions.

specimen, 2% drift ratio was adopted as the reference displacement for defining the CUREE protocol used during the quasi-static test program.

Fig. 9 shows the wall local response for earthquake test EQ4: DE, which targeted a design-level performance. This figure documents the end of the wall segment uplift, tie-rod forces F^t, and wall shear distortion γ compared with the global drift ratio and lateral force histories. Comparing wall lateral drift with the end of wall uplift, as the wall moved toward the east (positive) direction, wall uplift was observed on the west ends of both shear wall segments, and the east ends of the shear segments bore into the bottom HSS. Similarly, when the wall drift was to the west (negative) direction, uplift on the east ends of both shear wall segments and bearing in compression on the west ends of the shear wall segments was observed. The circles represent the time instances when each response parameter attains its peak values in positive drift and negative drift direction. It can be observed that the time instances of peak measurement for these responses occur simultaneously with peak global drift and lateral force.

The axial force response of the tension tie-rods was quite similar to wall uplift measurements with respect to wall drift in the positive and negative direction because those uplift measurements were located near the tension rod locations. Notably, all tie-rod forces remained below 20% yield strength. However, all rods reported a low axial force when its surrounding stud packs were expected to be in compression. Tension rods placed closer to the ends of walls consistently reported larger axial forces compared to rods placed toward the interior of the walls. This indicates that the two shear wall segments did not behave strictly as individual Type I segments. This observation is inconsistent with the tension tie-rod behavior observed in a prior full-scale building shake table test program (Wang and Hutchinson 2021). This discrepancy may be attributed to the different wall boundary elements in the two test programs. Namely, in the present program, the concrete mass at the top of the in-line wall specimens essentially acted as a rigid floor diaphragm. In contrast, a CFS floor system in the building tests of Wang and Hutchinson (2021) offered nominal diaphragm flexibility. Additionally, the wall layout and wall end boundary conditions were significantly different in the building test, which may have also affected the local behavior. Additionally, the tension rods experienced pretension loss due to repetitive shaking. The rods were pretensioned prior to the shaking sequence; however, due to the subsequent seismic motion, invariably a reduction in pretension occurred during the tests.

The measured panel distortion of different segments of the wall in both directions are also presented in Fig. 9. It can be seen that the gravity wall segment underwent 1.8–2.3 times larger panel distortion compared with its adjacent shear wall segments because kinematic constraints were maintained between them. The shear distortion histories of the two shear wall segments show that even though they drifted the same amount laterally, the two segments did not undergo the same amount of shear distortion, uplift, and

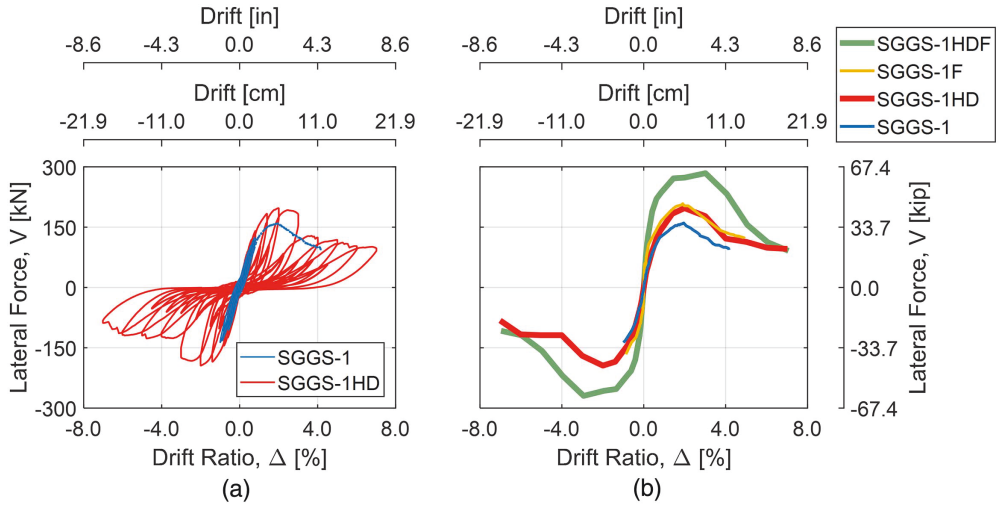

Fig. 10. Effect of tie-down detailing: (a) force-displacement response; and (b) backbone curve comparison.

Table 5. Effect of tie-down detailing: results summary

Test phase	Specimen	Wall strength, V_u (kN)	Drift ratio at $0.4V_u$ (prepeak), $\Delta_{0.4Vu}$ (%)	Drift ratio at V_u (peak), Δ_{Vu} (%)	Drift ratio at $0.8V_u$ (postpeak), $\Delta_{0.8Vu}$ (%)	Elastic stiffness,[a] K (kN/cm)
Shake table	SGGS-1	160.2	0.28	1.95	2.79	84.5
		—	−0.29	—	—	81.5
	SGGS-1F	208.2	0.15	1.90	3.14	205.9
		—	−0.13	—	—	237.1
Quasi-static	SGGS-1HD	197.4	0.35	1.99	3.36	82.9
		−194.3	−0.32	−2.00	−3.57	89.5
	SGGS-1HDF	284.7	0.17	3.01	4.13	237.3
		−269.2	−0.18	−2.94	−4.03	223.9

[a]When information about wall strength was not available in the negative direction, for stiffness calculations, the strength was assumed to be the same as the positive direction; 1 kN = 0.225 kip; and 1 kN/cm = 0.57 kip/in.

stud/track bending. The east shear wall segment underwent greater shear distortion when the wall drift was eastward, whereas the west shear wall segment underwent greater shear distortion when the wall drift was westward.

This was also similarly observed in the contribution of wall uplift to its lateral drift. When the wall drift was eastward, there was a larger contribution of wall uplift to the lateral drift for the west shear wall segment, and hence, lower shear distortion. These relative contributions of shear distortion and wall uplift to lateral drift for all segments evolved as specimen damage progressed. Similarly, the wall lateral resistance was influenced by the tension tie-rod axial forces. The evolution of these responses for different specimens will be discussed in subsequent sections.

Effect of Tie-Down Detailing

As mentioned, most wall configurations tested during the experimental program used tension tie-rods for shear wall detailing, either of the Type I or Type II configurations. However, prior experimental programs on CFS-framed shear walls has generally involved use of hold-downs as the tie-down systems. Thus, it was considered important to include configurations in the test matrix, which compared the effect of these two different tie-down details on wall behavior. Two configurations, namely SGGS-1HD (unfinished) and SGGS-1HDF (finished), in the quasi-static test phase used hold-downs instead of tension tie-rods. Fig. 10(a) shows the force-displacement response comparison between wall Specimens SGGS-1 (tension tie-rods) and SGGS-1HD (hold-downs), and Table 5 summarizes important response measurements.

These results show that specimens detailed with tie-rods compared with nominally identical specimens detailed with hold-downs demonstrated considerably lower strength and moderately lower stiffness, irrespective of the presence of finish or not. Notably, however, the drift at which strength was achieved was similar for the two specimens. The exception to this was the finished Specimen SGGS-1HDF, which attained strength at 3.0% drift ratio, as seen from the backbone curves in Fig. 10(b). The elastic stiffness of the walls with tension tie-rods was slightly lower (5%) than similarly framed specimens with hold-downs on average. Specimens with hold-downs also demonstrated 20%–30% larger lateral strength. This is mostly attributed to the 20% larger overturning moment lever arm provided when hold-downs were utilized because they were placed outside of the chord stud packs. In contrast, tie-rods were sandwiched between the chord stud packs, and hence, had a smaller overturning moment lever arm.

Prior to 2% drift ratio, damage to the specimen was limited to the steel sheet and the screws connecting the sheet to wall framing. Most of the screw damage was concentrated around the corners of the sheet. No damage to framing members was observed up to these drift demands. This was followed by sheet pullover around 4% drift ratio. This damage was similar to that observed in specimens with tension tie-rods. However, between 3% and 4% drift ratios, significant damage to the hold-downs at the wall ends was observed due to prying action at the anchor rod centerline leading to a weld failure. Fig. 11 shows the damage to the hold-downs at 4% drift ratio.

Between 4% and 7% drift ratio, several hold-down anchor rods failed as they experienced excessive tie-down forces, beyond their ultimate capacity. In contrast, the tie-rods remained linear-elastic when the specimens with tension rods were subjected to similar drift demands. This is of particular concern because the hold-downs and tie-rods were designed for the same overstrength level forces $\Omega_o = 3.0$ (Singh et al. 2020a). A pair of hold-downs having a combined nominal capacity ($2 \times F_u$) of 400 kN were installed at every chord stud pack location. Despite this, several hold-downs suffered extensive damage. Furthermore, the two hold-downs installed on the same stud pack did not experience equal amounts of force. Due to the difference in the overturning lever arm, there was an imbalance in the load sharing between the two hold-downs, with the outer most hold-down experiencing significantly larger axial forces. As seen in Fig. 11(e), the outer hold-down was already experiencing more then 50% of its individual nominal capacity and three to four times larger force compared with the other hold-down before the specimen reached strength. It is expected that due to this imbalance, the outer hold-downs on both ends of the

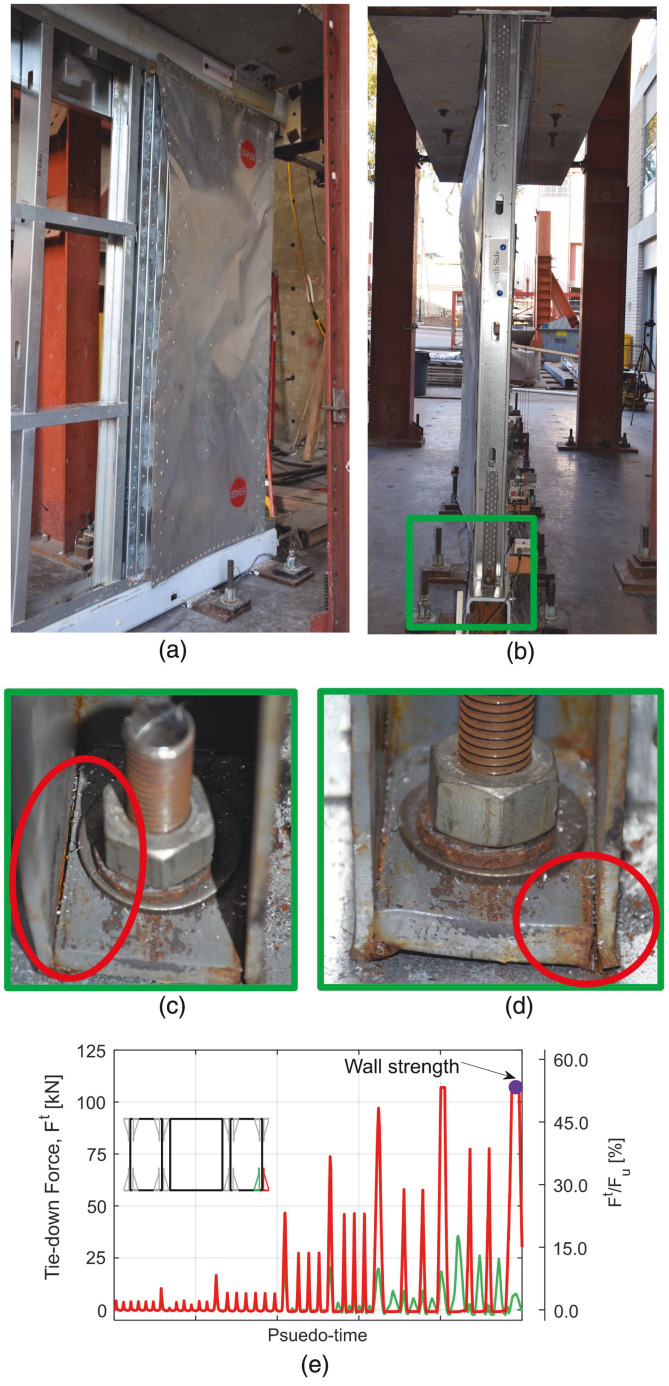

Fig. 11. (a–d) Damage to steel sheet and hold-downs used in Specimen SGGS-1HD at drift ratio $\Delta = 4.0\%$; and (e) tie-down force time history of hold-downs installed on stud pack.

wall reached their capacity earlier and failed during the large drift demand cycles.

Fig. 12 shows the comparison of tie-down force evolution between two pairs of wall configurations, one employing hold-downs and the other employing tension tie-rods, with increasing lateral force (V/V_u) and lateral drift (Δ/Δ_{Vu}). The compression-only button-type load cells employed for measuring hold-down forces were precompressed before beginning of test. During cyclic testing, some of the hold-downs became loose, which showed up as negative tie-down force in Fig. 12. In addition, for each measurement, response in only the direction of interest (push or pull) has been shown through indicated traces, and response in the other direction is grayed out. Schematics indicate location and type of response plotted.

Similar to what was observed from damage to SGGS-1HD, hold-downs experienced significantly larger axial forces compared with tension tie-rods. With eight hold-downs connected to the bottom transfer beam, wall configurations employing hold-downs had a more rigid connection to the base compared with wall configurations with tie-rods, which had only four such connections. As a result, the wall end uplift was significantly lower when hold-downs were employed. This also explains the panel shear distortion evolution of the shear segments. Because the contribution toward drift due to uplift is low for walls with hold-downs, the contribution of panel shear distortion to the drift Δ^{γ} is higher. These can be seen by studying Fig. 13, which shows the comparison of panel shear distortion evolution of the shear segments between the same pairs of wall configurations, with increasing lateral force and lateral drift.

Effect of Shear Wall Detailing

Among the 16 wall configurations tested, five configurations were detailed as Type II shear walls. Consistent with AISI S400-15 (AISI 2015b), tie-downs and compression posts for Type II shear walls were provided at the ends of the wall only. However, these Type II specimens were not designed and detailed with any members collecting and carrying the shear to the shear wall segments at the ends. As such, these specimens were not code-compliant Type II shear walls as defined in AISI S400-15 (AISI 2015b). Nonetheless, they shared the most salient characteristic of Type II walls.

Fig. 14 shows the force-displacement response comparison between wall Specimens SGGS-1 and SGGS-2, and Table 6 summarizes important response measurements. From this figure, it can be seen that the Type II specimen achieved about 30% lower strength when compared with the Type I specimen. Additionally, the drift at which strength was achieved, as well as the elastic stiffness, was also lower for the Type II specimen.

Fig. 14 also shows the backbone curves of three Type II wall configurations compared with a similarly framed Type I wall configurations (total of six specimen backbone curves). These aggregate backbone curve comparisons consistently demonstrate that the Type II specimens had about 70% of the strength of a similarly

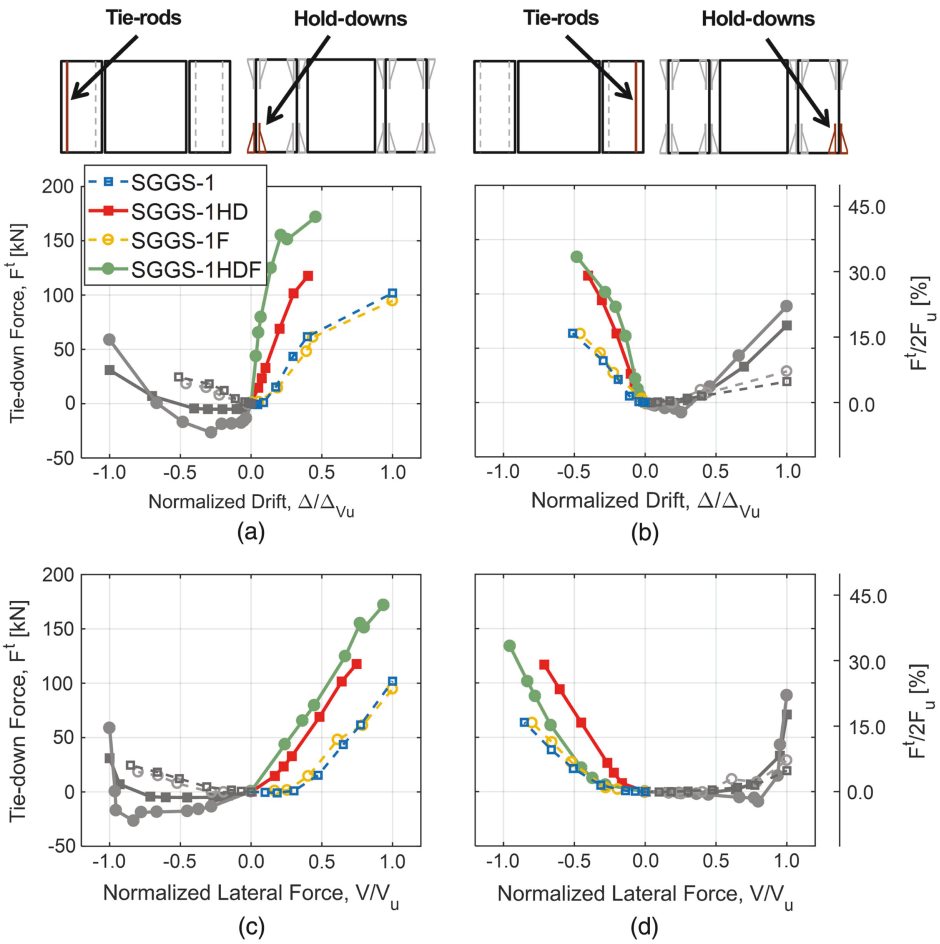

Fig. 12. Effect of tie-down detailing on anchor forces with increase in (a and b) normalized drift; and (c and d) normalized lateral force. Plots (a and c) present results for the left wall end tie-down, and plots (b and d) present results for the right wall end tie-down.

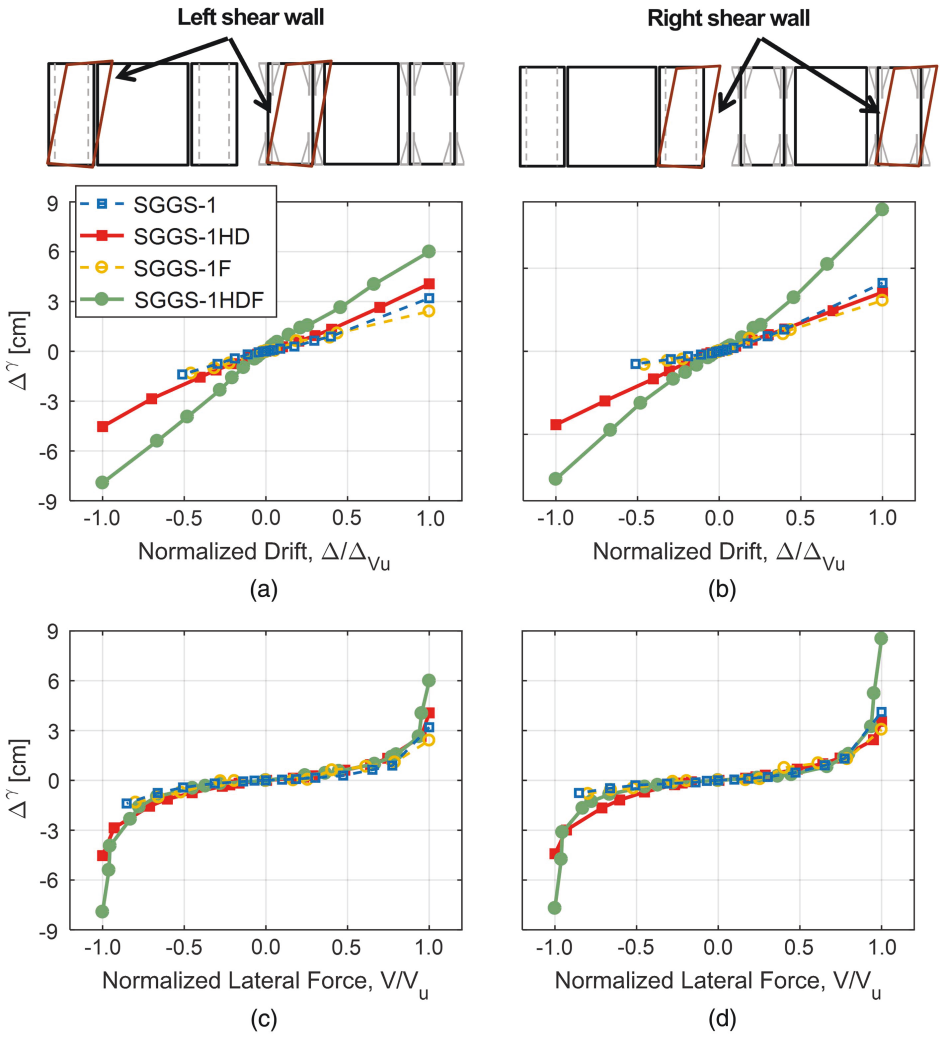

Fig. 13. Effect of tie-down detailing on shear wall shear distortion with increase in (a and b) normalized drift; and (c and d) normalized lateral force. Plots (a and c) present results for the left shear wall, and plots (b and d) present results for the right shear wall.

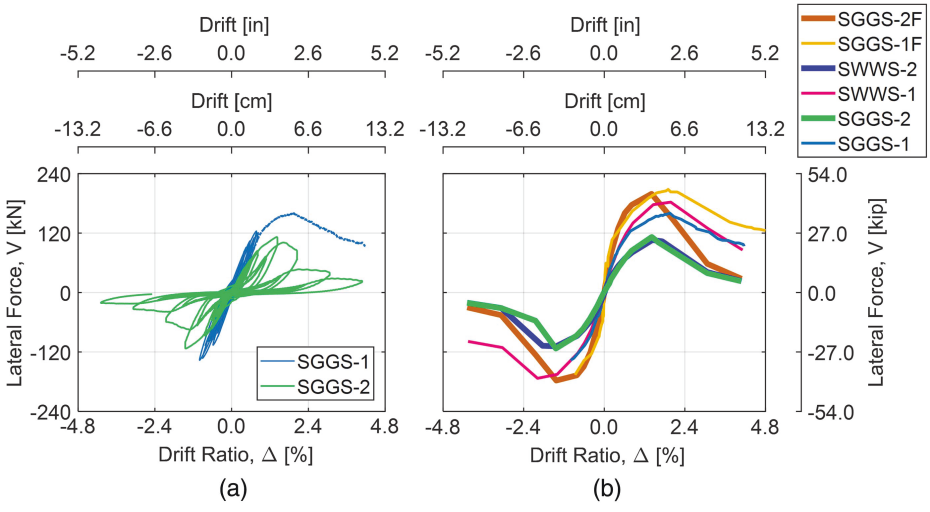

Fig. 14. Effect of shear wall detailing: (a) force-displacement response; and (b) backbone curve comparison.

framed Type I wall, on average. Elastic stiffness for a Type II wall was also similarly about 60% of the elastic stiffness of a similarly framed Type I wall, on average. Drift at strength for Type II walls was always lower than its Type I counterpart.

Specifically, for specimens tested within the shake table test phase, for the Type II Specimen SGGS-2B, the accumulation of damage through the earthquake test sequence led to an elongation of the fundamental period from 0.180 s in its undamaged state to

Table 6. Effect of shear wall detailing: results summary

Test phase	Specimen	Wall strength, V_u (kN)	Drift ratio at $0.4V_u$ (prepeak), $\Delta_{0.4V_u}$ (%)	Drift ratio at V_u (peak), Δ_{V_u} (%)	Drift ratio at $0.8V_u$ (postpeak). $\Delta_{0.8V_u}$ (%)	Elastic stiffness, K (kN/cm)
Shake table	SGGS-1	160.2	0.28	1.95	2.79	84.5
		—	−0.29	—	—	81.5
	SGGS-2B	84.1	0.17	1.22	1.77	70.7
		−73.8	−0.15	−0.79	−1.39	70.7
	SGGS-1F	208.2	0.15	1.90	3.14	205.9
		—	−0.13	—	—	237.1
Quasi-static	SGGS-2	113.3	0.36	1.41	1.89	46.2
		−111.8	−0.37	−1.44	−1.68	44.4
	SGGS-2F	199.2	0.20	1.41	1.90	141.9
		−177.7	−0.21	−1.43	−1.85	121.7
	SWWS-1	182.5	0.34	1.97	2.74	79.1
		−173.3	−0.36	−2.00	−2.58	70.4
	SWWS-2	107.2	0.30	1.43	2.13	52.6
		−107.3	−0.29	−1.43	−2.17	54.1
	SWWS-2F	181.8	0.29	2.01	2.66	91.9
		−169.0	0.29	−1.42	−2.41	84.7

Note: 1 kN = 0.225 kip; and 1 kN/cm = 0.57 kip/in.

0.327 s following the design-level earthquake test compared with the Type I Specimen SGGS-1 for which period elongation ranged from 0.157 to 0.199 s, and the Type I Specimen with finishes SGGS-1F for which period elongation ranged from 0.082 to 0.201 s. Similarly, the damping ratio for SGGS-2B increased from 2.5% in its undamaged state to 11.5% after the design-level earthquake test, compared with SGGS-1 and SGGS-1B, for which the damping ratio changed from 2.1% to 5.3% and from 3.3% to 7.9%, respectively.

Due to the reduced tension tie-rods and steel sheet fasteners, the Type II specimens were naturally anticipated to have a lower strength and stiffness. For such Type II walls, AISI S400-15 (AISI 2015b) suggests a 50% reduction in lateral strength. However, experimental results indicated that these reductions were not as high as suggested by the code. Both Type I and Type II walls had similar failure modes, namely widening of tension field action with increased drift demand causing tilting/bearing around screw heads, eventually leading to sheet pullover the screw heads. However, the sheet pullover was observed at a much earlier drift ratio, approximately 2% drift ratio for Type II walls.

Fig. 15 shows the comparison of tension tie-rod force evolution between two Type II and Type I wall configuration pairs, (1) SGGS-2 and SGGS-1; and (2) SWWS-2 and SWWS-1, with increasing lateral force and lateral drift. For the same amount of lateral force, tension rods in Type II specimens experienced larger axial forces when compared with Type I specimens. Because of the lower number of steel sheet fasteners in Type II walls, a greater portion of lateral force has to flow through the tension tie-rods. However, when normalized for lateral force or drift at strength, Type I specimens showed higher axial forces. Due to higher stiffness, Type I specimens experienced higher lateral force compared with Type II specimens for the same normalized lateral drift, which shows up as greater axial force in the tension tie-rods. Comparison of wall end uplift evolution between Type II and Type I wall specimens with increase in lateral force and lateral drift remained consistent with tension tie-rod forces. Type II specimens experienced greater wall uplift compared with Type I specimens for the same lateral force because Type II specimens had lower stiffness. However, when normalized for lateral force or drift at strength, Type I specimens showed greater wall uplift.

A comparison of panel shear distortion evolution of the shear segments between the same pairs of Type II and Type I wall configurations with increase in lateral force and lateral drift showed that for the same lateral force, the different segments of Type II specimens underwent greater panel distortion compared with Type I specimens. This was expected because Type II specimens have lower stiffness. However, after normalizing for individual lateral force at strength, the differences were not as significant, with distortion in Type I specimens being slightly higher only at high applied lateral forces. Looking at this evolution in terms of growth in normalized lateral drift, the difference in wall stiffness explains the greater panel distortion in Type I specimens.

Effect of Sheet Fastener Pattern

Yu et al. (2007) reported that using a staggered screw pattern for attaching the steel sheet to built-up chord stud members of (Type I) shear walls improved their shear strength. However, there is a lack of experimental data regarding the variation of screw pattern on shear walls that use stud packs as boundary element. Due to this, one wall configuration (SGGS-1XS) with an alternative sheet fastener pattern was added to the shake table test matrix. Generally, for all Type I configurations, the steel sheet was attached to the shear wall framing with 51-mm (or 102-mm staggered) o.c. spacing at the outer chord stud packs and 305-mm o.c. spacing at the field stud and interior chord stud packs. For SGGS-1XS, the steel sheet was attached to the shear wall framing with 51-mm o.c. spacing at the outer and inner chord stud packs and 305-mm o.c. spacing at the field stud. This difference is shown in Figs. 16(a and b).

Steel Framing Alliance (1997) documented results from tests on Type II CFS shear walls with varying sheathing area, finding walls with higher sheathing area demonstrated higher strength. However, there are no experimental data on the variation of fastener spacing along the edge of steel sheet adjacent to any perforations, or in this case, next to a gravity bay. Generally, for all Type II configurations, the steel sheet was attached to the shear wall framing with 51-mm (or 102-mm staggered) o.c. spacing at the outer chord stud pack, 305-mm o.c. spacing at the field stud, and 102-mm o.c. at the chord stud (not a built-up member) located at the interior edge of steel sheet. For SGGS-2B, the steel sheet was attached to the shear wall

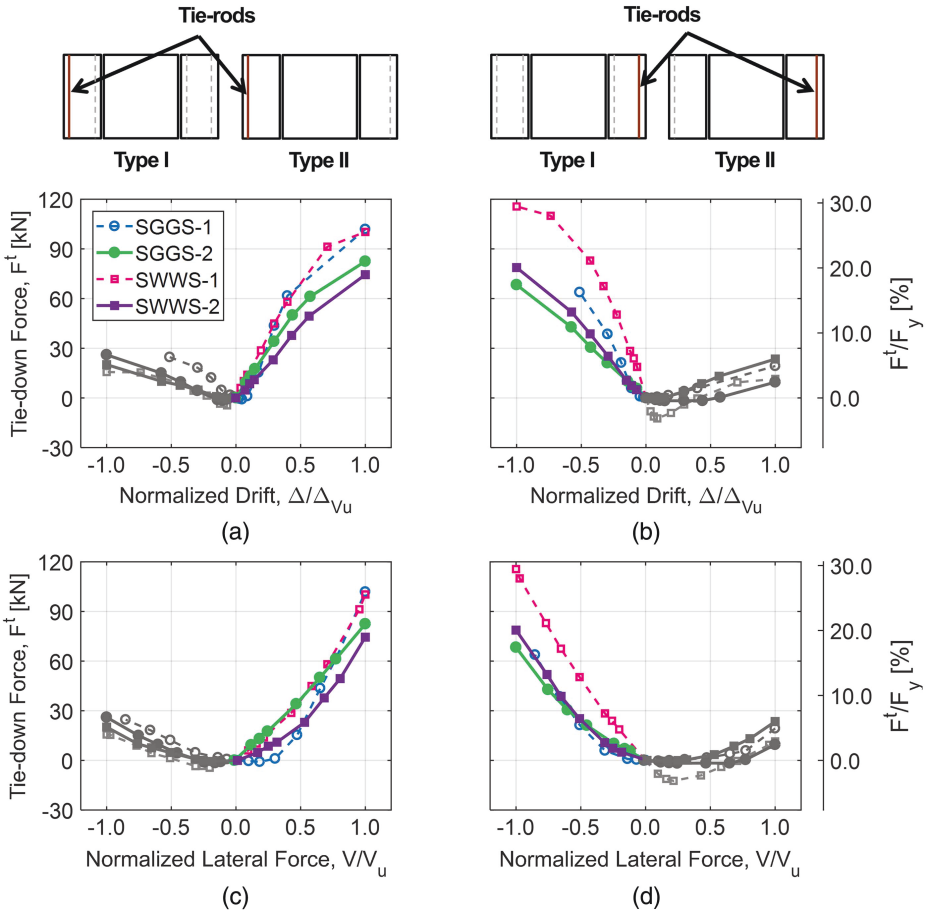

Fig. 15. Effect of shear wall detailing on tension-rod forces with increase in (a and b) normalized drift; and (c and d) normalized lateral force.

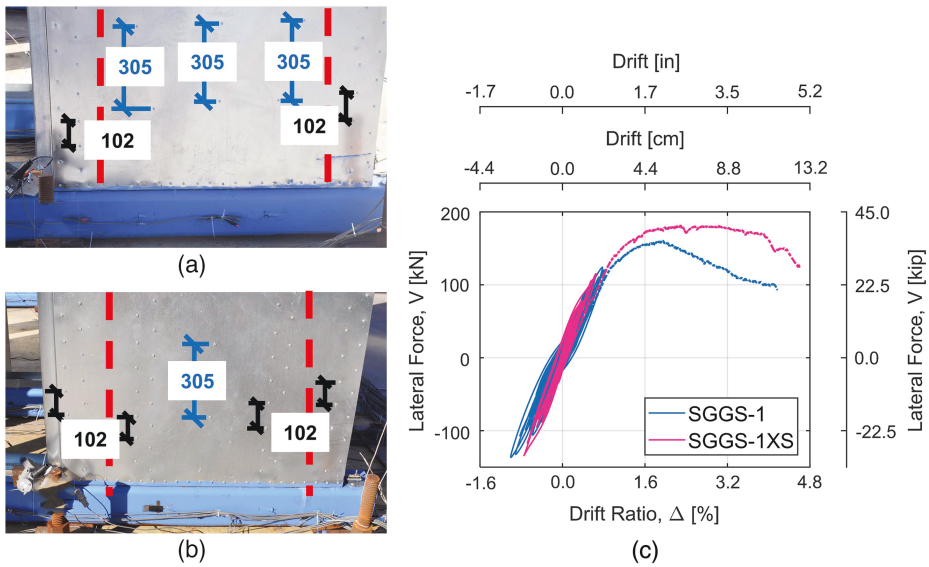

Fig. 16. Sheet fastener pattern for (a) SGGS-1; (b) SGGS-1XS (all units in mm); and (c) force-displacement response of SGGS-1 and SGGS-1XS. Field spacing in blue, and edge spacing in black font.

framing with 51-mm o.c. spacing at the outer chord stud pack, and 305-mm o.c. spacing at the field stud and the chord stud located at the interior edge of steel sheet. This difference is shown in Figs. 17 (a and b).

Figs. 16(c) and 17(c) show the force-displacement curve comparisons between configurations SGGS-1 and SGGS-1XS and between configurations SGGS-2 and SGGS-2B. It can be seen from the hysteresis response in both cases that the use of additional

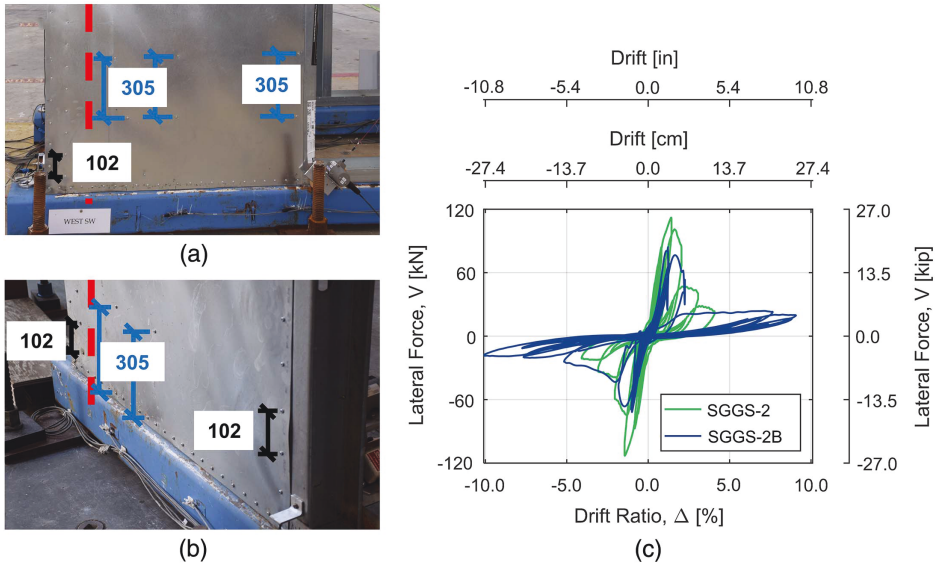

Fig. 17. Sheet fastener pattern for (a) SGGS-2B; (b) SGGS-2 (all units in mm); and (c) force-displacement response of SGGS-2 and SGGS-2B. Field spacing in blue, and edge spacing in black font.

fasteners for attaching steel sheet led to increase in specimen strength and elastic stiffness. SGGS-1XS showed a modest 13% increase in strength and 8% increase in elastic stiffness over SGGS-1. However, the presence of additional screws increased the drift at strength for the SGGS-1XS specimen up to 2.29%, from 1.95% for SGGS-1.

The postpeak strength drop behavior was also significantly different due to the larger number of fasteners being engaged. Specimen SGGS-1XS demonstrated an elongation of the fundamental period from 0.143 s in its undamaged state to 0.171 s following the design-level earthquake test, which was similar to Specimen SGGS-1, for which period elongation ranged from 0.157 to 0.199 s. The damping ratio for SGGS-1XS increased from 1.6% to 3.3%, similar to SGGS-1, for which damping ratio changed from 2.1% to 5.3%. Further discussion on evolution of dynamic characteristics for specimens tested during the shake table test phase have been given by Singh et al. (2020b).

Fig. 18 compares the damage to the steel sheet and fasteners at the end of monotonic pull tests for both the specimens. In both cases, steel sheet screws governed the wall response. Using more screws did not lead to change in the failure mode. Wall local behavior such as tension tie-rod forces also remained similar between the two configurations.

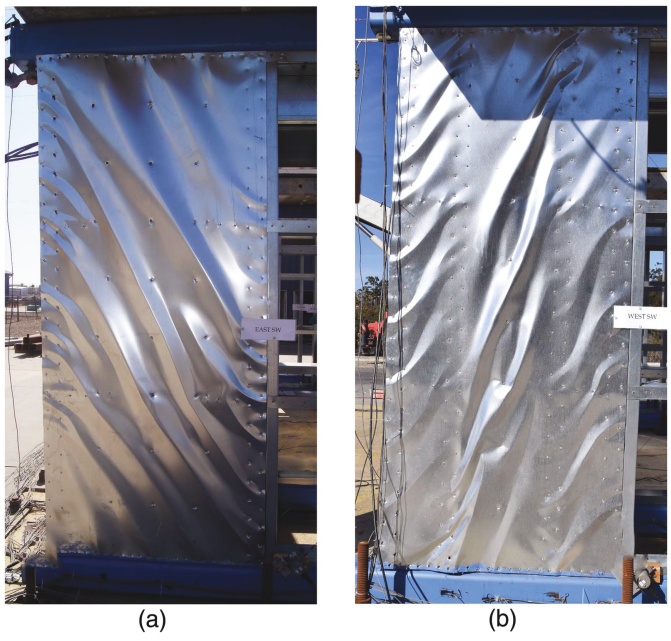

Fig. 18. Damage to steel sheet and fasteners at the end of monotonic pull tests for (a) SGGS-1 ($\Delta_{max} = 4.15\%$ and $\Delta_{res} = 1.85\%$); and (b) SGGS-1XS ($\Delta_{max} = 4.60\%$ and $\Delta_{res} = 2.79\%$).

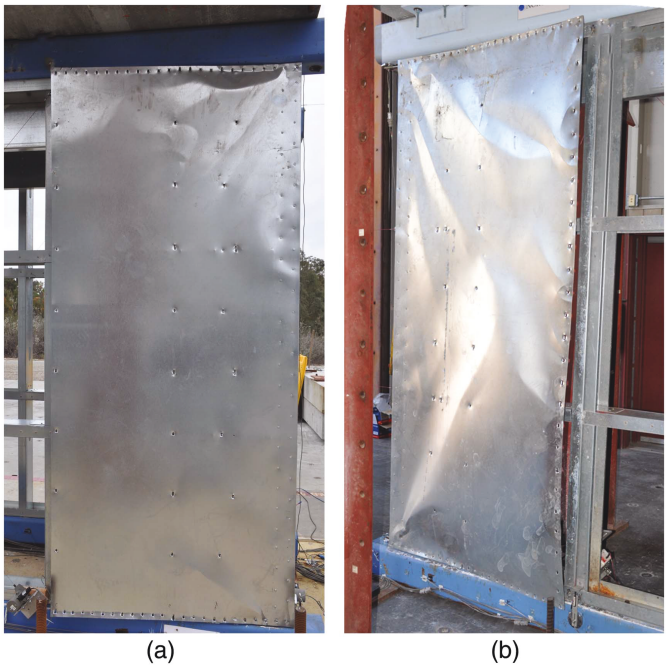

Fig. 19. Damage to steel sheet and fasteners at the end of testing for (a) SGGS-2B ($\Delta_{max} = 10.0\%$ and $\Delta_{res} = -0.23\%$); and (b) SGGS-2 ($\Delta_{max} = 4.08\%$).

Table 7. Effect of sheet fastener pattern: results summary

Test phase	Specimen	Wall strength, V_u (kN)	Drift ratio at $0.4V_u$ (prepeak), $\Delta_{0.4V_u}$ (%)	Drift ratio at V_u (peak), Δ_{V_u} (%)	Drift ratio at $0.8V_u$ (postpeak), $\Delta_{0.8V_u}$ (%)	Elastic stiffness, K (kN/cm)
Shake table	SGGS-1	160.2	0.28	1.95	2.79	84.5
		—	−0.29	—	—	81.5
	SGGS-1XS	181.5	0.31	2.29	4.13	86.2
		—	−0.28	—	—	93.3
	SGGS-2B	84.1	0.17	1.22	1.77	70.7
		−73.8	−0.15	−0.79	−1.39	70.7
Quasi-static	SGGS-2	113.3	0.36	1.41	1.89	46.2
		−111.8	−0.37	−1.44	−1.68	44.4

Note: 1 kN = 0.225 kip; and 1 kN/cm = 0.57 kip/in.

A 30% reduction in lateral strength was observed for SGGS-2B compared with SGGS-2. Drift at strength for SGGS-2B was also lower at 1.22%, compared with 1.41% for SGGS-2. The postpeak behavior was quite similar because the failure mode for both specimens was bearing/tilting or tearing around fastener heads leading to eventual sheet pull over fastener heads. Fig. 19 shows the damage to the steel sheet and fasteners at the end of their respective tests, with full-height steel sheet pull over fastener heads along the edge with coarser fastener edge spacing. A summary of the important response measurements is provided in Table 7.

Conclusions

To advance the understanding of CFS-framed steel sheet sheathed shear walls placed in-line with gravity walls, a two-phased experimental program was undertaken. Eight pairs of wall configurations were tested at full scale under a sequence of increasing amplitude earthquake motions at the NHERI Large High-Performance Outdoor Shake Table at the University of California, San Diego. Ten single wall-line configurations were tested under quasi-static cyclic loading conditions at the University of California, San Diego, Structural Engineering Powell Laboratory. An overview of this unique CFS wall-line test program as distributed into the two test phases was presented in this paper. One of the main objectives of the experimental effort was to characterize the performance of long CFS-framed walls, with particular interest in CFS walls detailed for midrise to high-rise construction in high intensity seismic zones. The test matrices were designed to also examine the impact of several variables on wall behavior. Of those test variables, the impact of variables governing the structural detailing of CFS-framed walls, namely tie-down detailing, shear wall detailing, and sheet fastener detailing, has been discussed in this paper, and the main findings are summarized here:

1. Tie-down detailing:
   - Specimens with hold-downs demonstrated 20%–30% larger lateral strength. This was because installation of hold-downs led to a larger overturning lever arm compared with tension tie-rods.
   - Several hold-downs reached their capacity at higher drift demands whereas tension tie-rods remained linear elastic even though both were designed for same overstrength force levels.
   - The difference in the overturning lever arm led to an imbalance in load sharing between the pair of hold-downs installed on the same stud pack. It is expected that this led to the outer hold-down reaching its nominal capacity earlier and failing.
   - The lateral capacity of shear walls can often be limited due to hold-down capacity available for design. Such an issue is usually not encountered when designing with tension tie-rods, which offer increased flexibility to the wall system.
2. Shear wall detailing:
   - Type II specimens had approximately 60% lower strength compared with similarly framed Type I specimens. This was due to the reduced number of tension rods and steel sheet fasteners used. However, the reduction in lateral strength was not as large as suggested by AISI S400-15 (AISI 2015b).
   - The elastic stiffness was 65% lower for Type II specimens. Drift at strength was also consistently lower for Type II specimens compared with Type I specimens.
3. Sheet fastener pattern:
   - Use of additional fasteners for steel sheet installation led to a modest increase in strength, stiffness, and drift at strength.
   - Fastener detailing change did not alter local wall response measurements or observed physical failure mode.

Results from this test program enrich the experimental database by documenting the performance of CFS-framed wall assemblies, and in particular addressing shear walls placed in-line with gravity walls. Outcomes pertaining to the impact of structural detailing design variables on wall performance add valuable information to the ongoing development of seismic systems for buildings framed with CFS. Similarly, the companion paper (Singh et al. 2022b) explores the impact of nonstructural detailing on steel sheet sheathed CFS wall-lines and provides insight into the effects of architectural finishes and window openings on wall performance.

Data Availability Statement

The specimens tested under the CFS-NHERI experimental program were monitored with many analog sensors in addition to digital still cameras, several video cameras, and GPS and UAV monitoring systems. High-quality data generated during the study are publicly available within the DesignSafe-CI repository (Singh et al. 2021a, 2022a).

Acknowledgments

The research presented herein is funded through the National Science Foundation (NSF) Grant Nos. CMMI 1663569 and CMMI 1663348, project entitled *Collaborative Research: Seismic Resiliency of Repetitively Framed Mid-Rise Cold-Formed Steel Buildings*. Ongoing research is a result of collaboration between three

academic institutions: University of California, San Diego, Johns Hopkins University, and University of Massachusetts, Amherst, two institutional granting agencies: American Iron and Steel Institute and Steel Framing Industry Association and 10 industry partners. Industry sponsors include ClarkDietrich Building Systems, California Expanded Metal Products Co. (CEMCO), SWS Panel, SureBoard, United States Gypsum Corporation (USG), MiTek, Nevell Group, Atlas Tube, the Steel Network (TSN), and NBM Technologies; who each provided financial, technical, construction, and materials support. Specific individuals that dedicated significant time on behalf of this effort included Greg Ralph (ClarkDietrich), Fernando Sesma (CEMCO), Diego Rivera (SWS Panels), Tyler Elliot (SureBoard), Shahab Torabian (NBM Technologies), Esmaeel Rahmani and Jesse Karnes (MiTek), and Mike Korthals and Mark Wilson (Nevell Group). Regarding support for the test programs, the efforts of NHERI@University of California, San Diego, and Powell Labs staff, namely, Noah Aldrich, Robert Beckley, Jeremy Fitcher, Abdullah Hamid, Dr. Christopher Latham, Darren McKay, Andrew Sander, Michael Sanders, and Alex Sherman, graduate students Filippo Sirotti and Maryam Soltani (University of Bologna, Italy), and several undergraduate students are greatly appreciated. Findings, opinions, and conclusions are those of the authors and do not necessarily reflect those of the sponsoring organizations.

Notation

The following symbols are used in this paper:

Ds_{5-95} = strong motion duration (s);
F^t = transient tie-down axial force (kN);
F_u = nominal capacity of a hold-down (kN);
F_y = tension tie-rod measured yield strength (kN);
g = gravitational acceleration constant (m/s^2);
K = elastic stiffness (kN/cm);
M_w = moment magnitude;
R_{rup} = rupture distance (km);
S_a = elastic psuedoacceleration spectra (g);
V = lateral force (kN);
V_{target} = percentage of wall strength (%);
V_u = wall strength (kN);
W = seismic weight (kN);
Δ = drift ratio (%);
Δ_{max} = maximum drift ratio (%);
Δ_{res} = residual drift ratio (%);
Δ_{target} = percentage of drift ratio at strength (%);
Δ_{Vu} = drift ratio at strength (%);
$\Delta_{0.4Vu}$ = drift ratio at 40% strength (prepeak) (%);
$\Delta_{0.8Vu}$ = drift ratio at 80% strength (postpeak) (%);
Δ^{γ} = contribution of shear distortion towards lateral drift (cm);
Ω_o = overstrength factor;
γ = shear distortion (%);
ξ = damping ratio (%); and
ϕ = rod diameter (mm).

References

AISI (American Iron and Steel Institute). 2015a. *North American standard for cold-formed steel structural framing*. AISI S240-15. Washington, DC: AISI.

AISI (American Iron and Steel Institute). 2015b. *North American standard for seismic design of cold-formed steel structural systems*. AISI S400-15. Washington, DC: AISI.

AISI (American Iron and Steel Institute). 2016. *North American specification for the design of cold-formed steel structural members*. AISI S100-16. Washington, DC: AISI.

ASTM. 2014. *Standard specification for structural bolts, steel, heat treated, 120/105 ksi minimum tensile strength*. ASTM A325-14. West Conshohocken, PA: ASTM.

ASTM. 2017. *Standard specification for steel sheet, zinc-coated (galvanized) or zinc-iron alloy-coated (galvannealed) by the hot-dip process*. ASTM A653/A653M-17. West Conshohocken, PA: ASTM.

ASTM. 2018. *Standard specification for cold-formed welded and seamless carbon steel structural tubing in rounds and shapes*. ASTM A500/A500M-18. West Conshohocken, PA: ASTM.

Balh, N., J. DaBreo, C. Ong-Tone, K. El-Saloussy, C. Yu, and C. Rogers. 2014. "Design of steel sheathed cold-formed steel framed shear walls." *Thin-Walled Struct.* 75 (Oct): 76–86. https://doi.org/10.1016/j.tws.2013.10.023.

Briere, V., and C. Rogers. 2017. *Higher capacity cold-formed steel sheathed and framed shear walls for mid-rise buildings: Part 2*. Research Rep. No. RP17-6. Montréal: McGill Univ.

DaBreo, J., N. Balh, C. Ong-Tone, and C. Rogers. 2014. "Steel sheathed cold-formed steel framed shear walls subjected to lateral and gravity loading." *Thin-Walled Struct.* 74 (5): 232–245. https://doi.org/10.1016/j.tws.2013.10.006.

Hikita, K. 2006. "Impact of gravity loads on the lateral performance of light gauge steel frame/wood panel shear walls." Master's thesis, Dept. of Civil Engineering and Applied Mechanics, McGill Univ.

Krawinkler, H., F. Parisi, L. Ibarra, A. Ayoub, and R. Medina. 2001. *Development of a testing protocol for woodframe structures*. CUREE Publication No. W-02. Richmond, CA: Consortium of Universities for Research in Earthquake Engineering.

Ong-Tone, C. 2009. "Tests and evaluation of cold-formed steel frame/steel sheathed shear walls." Master's thesis, Dept. of Civil Engineering and Applied Mechanics, McGill Univ.

Rizk, R., and C. Rogers. 2017. *Higher strength cold-formed steel framed/steel shear walls for mid-rise construction*. Research Rep. No. RP17-4. Montréal: McGill Univ.

Santos, V., and C. Rogers. 2017. *Higher capacity cold-formed steel sheathed and framed shear walls for mid-rise buildings: Part 1*. Research Rep. No. RP17-5. Montréal: McGill Univ.

Schafer, B. W. 2011. "Cold-formed steel structures around the world: A review of recent advances in applications, analysis and design." *Steel Constr.* 4 (3): 141–149. https://doi.org/10.1002/stco.201110019.

Serrette, R. 1997. *Additional shear wall values for light weight steel framing*. Rep. No. LGSRG-1-97. Santa Clara, CA: Santa Clara Univ.

Shamim, I., J. DaBreo, and C. A. Rogers. 2013. "Dynamic testing of single- and double-story steel-sheathed cold-formed steel-framed shear walls." *J. Struct. Eng.* 139 (5): 807–817. https://doi.org/10.1061/(ASCE)ST.1943-541X.0000594.

Singh, A., T. Hutchinson, X. Wang, Z. Zhang, B. Schafer, F. Derveni, H. Castaneda, and K. Peterman. 2021a. "Wall line tests: Phase 1—Shake table tests." In *CFS-NHERI: Seismic resiliency of repetitively framed mid-rise cold-formed steel buildings*. Seattle: DesignSafe-CI. https://doi.org/10.17603/ds2-mvj8-8386.

Singh, A., T. Hutchinson, X. Wang, Z. Zhang, B. Schafer, F. Derveni, H. Castaneda, and K. Peterman. 2022a. "Wall line tests: Phase 2—Quasi-static tests." In *CFS-NHERI: Seismic resiliency of repetitively framed mid-rise cold-formed steel buildings*. Seattle: DesignSafe-CI. https://doi.org/10.17603/ds2-encf-vj32.

Singh, A., and T. C. Hutchinson. 2022. *Lateral response of cold-formed steel framed steel sheathed in-line wall systems detailed for mid-rise buildings. Part II: Quasi-static test phase*. Structural Systems Research Project. Rep. No. SSRP-19/06. La Jolla, CA: Univ. of California.

Singh, A., X. Wang, and T. C. Hutchinson. 2021b. *Lateral response of cold-formed steel framed steel sheathed in-line wall systems detailed for mid-rise buildings. Part I: Shake table test phase*. Structural Systems Research Project. Rep. No. SSRP-19/05. La Jolla, CA: Univ. of California.

Singh, A., X. Wang, S. Torabian, T. C. Hutchinson, K. D. Peterman, and B. W. Schafer. 2020a. "Seismic performance of symmetric unfinished CFS in-line wall systems." In *Proc., ASCE Structures Congress 2020*, 629–642. Reston, VA: ASCE. https://doi.org/10.1061/9780784482896.058.

Singh, A., X. Wang, Z. Zhang, F. Derveni, H. Castaneda, K. Peterman, B. Schafer, and T. Hutchinson. 2020b. "Lateral response of cold-formed steel framed steel sheathed in-line wall systems detailed for mid-rise buildings." In *Proc., Cold-Formed Steel Research Consortium Colloquium*. Baltimore: Johns Hopkins Univ.

Singh, A., X. Wang, Z. Zhang, F. Derveni, H. Castaneda, K. D. Peterman, B. W. Schafer, and T. C. Hutchinson. 2022b. "Steel sheet sheathed cold-formed steel framed in-line wall systems. II: Impact of nonstructural detailing." *ASCE J. Struct. Eng*. 148 (12): 04022194. https://doi.org/10.1061/(ASCE)ST.1943-541X.0003434.

Steel Framing Alliance. 1997. *Monotonic tests of cold-formed steel shear walls with openings*. Research Rep. No. RP97-1. Washington, DC: American Iron and Steel Institute.

Van Den Einde, L., et al. 2004. "Development of the George E. Brown Jr. network for earthquake engineering simulation (NEES) large high performance outdoor shake table at the University of California, San Diego." In *Proc., 13th World Conf. on Earthquake Engineering*. Vancouver, BC, Canada: World Conf. on Earthquake Engineering.

Wang, X., and T. Hutchinson. 2021. "Earthquake and postearthquake fire testing of a midrise cold-formed steel-framed building. II: Shear wall behavior and design implications." *J. Struct. Eng*. 147 (9): 04021126. https://doi.org/10.1061/(ASCE)ST.1943-541X.0003098.

Yu, C. 2010. "Shear resistance of cold-formed steel framed shear walls with 0.686 mm, 0.762 mm, and 0.838 mm steel sheet sheathing." *Eng. Struct.* 32 (6): 1522–1529. https://doi.org/10.1016/j.engstruct.2010.01.029.

Yu, C., H. Vora, T. Dainard, J. Tucker, and P. Veetvkuri. 2007. *Steel sheet sheathing options for CFS framed shear wall assemblies providing shear resistance*. Rep. No. UNT-G76234. Denton, TX: Univ. of North Texas.

Zhang, Z., and B. W. Schafer. 2020. *Test report: Cyclic performance of steel sheet connections for CFS steel sheet shear walls*. CFSRC Rep. No. R-2020-06. Baltimore: Johns Hopkins Univ.

Zhang, Z., A. Singh, F. Derveni, S. Torabian, K. Peterman, T. Hutchinson, and B. Schafer. 2021. "Cyclic experiments on isolated steel sheet connections for CFS framed steel sheet sheathed shear walls with new configurations." *Eng. Struct.* 244 (11): 112805. https://doi.org/10.1016/j.engstruct.2021.112805.